11th World Congress on Computational Mechanics (WCCM XI)
5th European Conference on Computational Mechanics (ECCM V)
6th European Conference on Computational Fluid Dynamics (ECFD VI)
E. Oñate, J. Oliver and A. Huerta (Eds)

A NUMERICAL INVESTIGATION ON THE HETEROGENEOUS AND ANISOTROPIC MECHANICAL BEHAVIOUR OF AISI H11 STEEL USING VARIOUS STRESS-STRAIN FORMULATIONS: A MULTI-SCALE APPROACH

Ahmed Zouaghi[*,†], **Vincent Velay**[*], **Adriana Soveja**[†] **AND Farhad Rézaï-Aria**[*]

[*] Université de Toulouse; INSA, UPS, Mines Albi, ISAE; ICA (Institut Clément Ader),
Campus Jarlard F-81013 Albi Cedex 09, France
e-mail: vincent.velay@mines-albi.fr; rezai@mines-albi.fr
Web page: http://www.institut-clement-ader.org/

[†]Université de Toulouse; INSA, UPS, Mines Albi, ISAE; ICA (Institut Clément Ader),
10 Avenue Edouard Belin, F-31055 Toulouse Cedex 4, France
e-mail: ahmed.zouaghi@isae.fr; adriana.soveja@isae.fr
Web page: http://www.institut-clement-ader.org/

Key words: multi-scale modelling, finite element, objective stress rate, localization, AISI H11 steel, heterogeneous materials

Abstract. In this paper, a numerical investigation is carried out on the heterogeneous and anisotropic mechanical behaviour of AISI H11 martensitic steel with a multi-scale approach. For this purpose, an elasto-viscoplastic model that considers nonlinear isotropic and kinematic hardenings is implemented in a finite element code using three stress-strain formulations: the small strain assumption where rotation is neglected; and two formulations based on finite strain theory in Eulerian framework which are respectively defined by the Jaumann-Zaremba and the Olroyd objective rates of Kirchhoff stress. The parameters of the constitutive equations are identified using macroscopic quasi-static and cyclic material responses and small strains assumption by the mean of a localization rule. By using particular Voronoï tessellations, a virtual realistic microstructure, consisting of laths and grains, is generated considering the specific crystallographic orientations α'/γ (martensitic/austenitic phases) relation (i.e. Kurdjumov-Sachs relation). Finite element computations are then performed on this virtual microstructure and exhibit that; besides laths orientations, morphologies and interactions; the full-field local mechanical fields are dependant on the used stress-strain formulation.

1 INTRODUCTION

During forming and machining processes, the surface of metallic structures are experiencing heterogeneous and anisotropic inelastic deformations which can lead to significant changes in the microstructure of the material. Since material properties and life assessment of metallic engineering structures are in concerns, it is thus important to better get insight into the local mechanical response by the mean of a multi-scale approach, i.e. how a global macroscopic load is accommodated at the local scale of a single grain. In this direction, several progresses have been made in the development of multi-scale materials models benefiting from the increase of computational resources [1, 2]. These approaches have been used to investigate mechanical fields localization prediction as a function of the parameters of the material microstructure; and show generally a quite satisfactory agreement with experimental observations [3, 4]. Nevertheless, the effects of the used stress-strain formulation on the local mechanical behaviour have not been investigated. It is well known that, besides small strain assumption, it is possible to use several finite strain formulations whether in Lagrangian or Eulerian framework for multi-scale modelling.

The aim of this work is to carry out a numerical investigation on the local heterogeneous and anisotropic mechanical response of AISI H11 martensitic steel using three various stress-strain formulations [5]: the basic small strain assumption where rotation is neglected; and two formulations based on finite strain theory in Eulerian framework which are respectively defined by the Jaumann-Zaremba and the Olroyd objective rates of Kirchhoff stress. For this purpose, the elasto-viscoplastic model of Méric and Cailletaud [1] is implemented in the finite element code ABAQUS using these formulations. The parameters of the constitutive equations are identified from experimental quasi-static and cyclic material reponses data by the mean of a scale transition rule [6]. Finite element computations are then performed on a virtual realistic microstructure that is generated by an adapted Voronoï tesselations where the specific crystallographic orientations α'/γ (martensitic/austenitic phases) relation (i.e. Kurdjumov-Sachs relation) is taken into account. This implies to get an accurate information about mechanical fields localization.

The paper is organized as follows. In the first part, the constitutive equations and the associated numerical integration scheme in the context of the investigated stress-strain formulations are outlined. Next, The identification of the multi-scale model parameters is given. The virtual microstructure and the associated crystallographic orientations generation are described in the third part. Finally, the last part is devoted to finite element computations and the obtained results.

2 MULTI-SCALE MODEL

2.1 Constitutive equations

The multi-scale model of Méric and Cailletaud [1] is formulated in the time dependent framework of continuum thermodynamics laws. The constitutive equations are written

at the lath scale and the associated variables are introduced at the slip system level. The shear strain rate $\dot{\gamma}^s$ on a system s is described by a power function. The accumulated shear strain is denoted by v^s:

$$\dot{\gamma}^s = sign(\tau^s - \chi^s)\,\dot{v}^s \tag{1}$$

$$\dot{v}^s = \left\langle \frac{\mid \tau^s - \chi^s \mid - r^s - \tau_0}{K} \right\rangle^n \tag{2}$$

where K and n are viscosity parameters, τ_0 is the initial critical resolved shear stress, r^s and χ^s are respectively the isoptropic and kinematic hardenings. The operator $\langle . \rangle$ denotes the Macaulay function. The kinematic and isotropic hardenings are nonlinear and are respectively associated to the internal state variables α^s and ρ^s as follows:

$$\chi^s = c\,\alpha^s \tag{3}$$

$$r^s = b\,Q \sum_r h_{sr}\rho^r \tag{4}$$

$$\dot{\alpha}^s = (sign(\tau^s - \chi^s) - d\,\alpha^s)\,\dot{v}^s \tag{5}$$

$$\dot{\rho}^s = (1 - b\rho^s)\,\dot{v}^s \tag{6}$$

where c and d are material parameters for kinematic hardening, Q and b are material parameters for isotropic hardening. The latter mechanism introduces a hardening matrix h_{sr} that describes the interaction between the overall slip systems to well capture the effect of dislocation densities. Knowing that the AISI H11 martensitic steel has a BCC structure, slip is assumed to occur on two slip systems sets: $\{110\}\langle 111\rangle$ and $\{121\}\langle 111\rangle$ for respectively easy and pencil glide. The corresponding hardening matrix is thus defined by eight coefficients h_i [7].

The present framework allows to work only on potentially activated slip systems sets and avoids complexe numerical procedures of time independent schemes. The expression of the resolved shear stress τ^s in (1) and (2) depends on whether finite strain theory is used or not. In this case (i.e finite strain theory), the resolved shear stress is given by:

$$\tau^s = \underset{\sim}{\boldsymbol{\tau}} : \underset{\sim}{\boldsymbol{m}}^s = det\underset{\sim}{\boldsymbol{F}}\,\underset{\sim}{\boldsymbol{\sigma}} : \underset{\sim}{\boldsymbol{m}}^s \tag{7}$$

where $\underset{\sim}{\boldsymbol{\tau}}$ and $\underset{\sim}{\boldsymbol{\sigma}}$ are respectively the Kirchhoff and Cauchy stress tensors, $\underset{\sim}{\boldsymbol{F}}$ is the transformation gradient and $\underset{\sim}{\boldsymbol{m}}^s$ is the symmetric part of the Schmid tensor defined as:

$$\underset{\sim}{\boldsymbol{m}}^s = \frac{1}{2}\left(\underline{\boldsymbol{l}}^s \otimes \underline{\boldsymbol{n}}^s + \underline{\boldsymbol{l}}^s \otimes \underline{\boldsymbol{n}}^s\right) \tag{8}$$

with $\underline{\boldsymbol{l}}^s$ and $\underline{\boldsymbol{n}}^s$ the slip direction and the normal to the slip plane respectively. Otherwise, in the case of small strain assumption, the expression of the resolved shear stress is simplified to:

$$\tau^s = \underset{\sim}{\boldsymbol{\sigma}} : \underset{\sim}{\boldsymbol{m}}^s \tag{9}$$

2.2 Constitutive problem and numerical scheme

The above constitutive equations are implemented in the finite element code ABAQUS using an implicit numerical integration scheme. The algorithm is based on the generalized trapezoidal rule θ-method [8] where shear strains γ^s are the primary integrated variables. The latter are involved in the return-mapping scheme of the elasto-viscoplastic constitutive probem:

$$\dot{\underset{\sim}{\boldsymbol{\tau}}} = \breve{\boldsymbol{\Lambda}} : \left(\underset{\sim}{\boldsymbol{D}}^{\mathbf{trial}} - \sum_{\mathbf{s}} \dot{\gamma}^{\mathbf{s}} \underset{\sim}{\boldsymbol{m}}^{\mathbf{s}} \right) \tag{10}$$

where $\breve{\boldsymbol{\Lambda}}$ is the fourth order tensor elastic moduli and $\underset{\sim}{\boldsymbol{D}}^{trial}$ is the trial symmetric rate part of the velocity gradient $\underset{\sim}{\boldsymbol{L}}$. Due to the inherent severe nonlinearilty of the problem, the resolution of the return-mapping equations is initially performed with the rate tangent modulus method developed by Peirce, Asaro and Needlman [9] before applying the Newton-Raphson iterative scheme.

As mentioned above, three stress-strain formuations are investigated [5]: the small strain assumption; and two formulations based on finite strain theory in Eulerian framework which are respectively defined by the Jaumann-Zaremba $\mathring{\underset{\sim}{\boldsymbol{\tau}}}^{J}$ and the Olroyd $\mathring{\underset{\sim}{\boldsymbol{\tau}}}^{O}$ objective rates of Kirchhoff stress. The latter one is derived from the Lagrangian framework and is given by:

$$\mathring{\underset{\sim}{\boldsymbol{\tau}}}^{O} = \dot{\underset{\sim}{\boldsymbol{\tau}}} - \underset{\sim}{\boldsymbol{L}} \,.\, \underset{\sim}{\boldsymbol{\tau}} - \underset{\sim}{\boldsymbol{\tau}} \,.\, \underset{\sim}{\boldsymbol{L}}^{T} \tag{11}$$

while the Jaumann-Zaremba objective rate of Kirchhoff stress is defined as:

$$\mathring{\underset{\sim}{\boldsymbol{\tau}}}^{J} = \dot{\underset{\sim}{\boldsymbol{\tau}}} - \underset{\sim}{\boldsymbol{W}} \,.\, \underset{\sim}{\boldsymbol{\tau}} - \underset{\sim}{\boldsymbol{\tau}} \,.\, \underset{\sim}{\boldsymbol{W}}^{T} \tag{12}$$

where $\underset{\sim}{\boldsymbol{W}}$ is the asymmetric spin part of $\underset{\sim}{\boldsymbol{L}}$. By introducing the above definitions in (10) and taking into account that ABAQUS employs the Jaumann-Zaremba stress rate, the constitutive elasto-viscoplastic problem is thus respectively for the Olroyd and Jaumann-Zaremba objective stress rates:

$$\mathring{\underset{\sim}{\boldsymbol{\tau}}}^{J} = \breve{\boldsymbol{\Lambda}} : \left[\underset{\sim}{\boldsymbol{D}}^{\mathbf{trial}} + \breve{\boldsymbol{\Lambda}}^{-\mathbf{1}} : \left(\underset{\sim}{\boldsymbol{D}}^{\mathbf{trial}} . \underset{\sim}{\boldsymbol{\tau}} + \underset{\sim}{\boldsymbol{\tau}} . \underset{\sim}{\boldsymbol{D}}^{\mathbf{trial}} \right) \right] - \sum_{\mathbf{s}} \left(\breve{\boldsymbol{\Lambda}} : \underset{\sim}{\boldsymbol{m}}^{\mathbf{s}} + \underset{\sim}{\boldsymbol{P}}^{\mathbf{s}} + \underset{\sim}{\boldsymbol{Q}}^{\mathbf{s}} \right) \dot{\gamma}^{\mathbf{s}} \tag{13}$$

$$\mathring{\underset{\sim}{\boldsymbol{\tau}}}^{J} = \breve{\boldsymbol{\Lambda}} : \underset{\sim}{\boldsymbol{D}}^{\mathbf{trial}} - \sum_{\mathbf{s}} \left(\breve{\boldsymbol{\Lambda}} : \underset{\sim}{\boldsymbol{m}}^{\mathbf{s}} + \underset{\sim}{\boldsymbol{Q}}^{\mathbf{s}} \right) \dot{\gamma}^{\mathbf{s}} \tag{14}$$

where $\underset{\sim}{\boldsymbol{P}}^{s}$ and $\underset{\sim}{\boldsymbol{Q}}^{s}$ are respectively given by:

$$\underset{\sim}{\boldsymbol{P}}^{s} = \underset{\sim}{\boldsymbol{m}}^{s} . \underset{\sim}{\boldsymbol{\tau}} + \underset{\sim}{\boldsymbol{\tau}} . \underset{\sim}{\boldsymbol{m}}^{s} \tag{15}$$

$$\underset{\sim}{\boldsymbol{Q}}^s = \underset{\sim}{\boldsymbol{w}}^s . \underset{\sim}{\boldsymbol{\tau}} - \underset{\sim}{\boldsymbol{\tau}} . \underset{\sim}{\boldsymbol{w}}^s \tag{16}$$

with $\underset{\sim}{\boldsymbol{w}}^s$ the asymmetric part of the schmid tensor:

$$\underset{\sim}{\boldsymbol{w}}^s = \frac{1}{2}\left(\underline{\boldsymbol{l}}^s \otimes \underline{\boldsymbol{n}}^s - \underline{\boldsymbol{l}}^s \otimes \underline{\boldsymbol{n}}^s\right) \tag{17}$$

When the small strain assumption is used, the elasto-viscoplastic constitutive problem takes the simplified form:

$$\underset{\sim}{\dot{\boldsymbol{\sigma}}} = \breve{\boldsymbol{\Lambda}} : \left(\underset{\sim}{\boldsymbol{D}}^{\mathbf{trial}} - \sum_{\mathbf{s}} \dot{\gamma}^{\mathbf{s}} \underset{\sim}{\boldsymbol{m}}^{\mathbf{s}}\right) \tag{18}$$

Besides the constitutive problem, other thermodynamical variables expressions involved in the return-mapping scheme depend on stress-strain formulations. This is the case for the resolved shear stress (7) which time derivative relies on these formulations. This would have consequences on the local mehcanical behaviour that are invetigated in section 5.

3 MATERIAL PARAMETERS IDENTIFICATION

The parameters identification is performed using experimental quasi-static and a strain controlled ($\Delta\epsilon/2 = 0.8\%$) cyclic material responses. The procedure consists to solve the inverse problem using small strain assumption and the β-rule scale transition model [6]. The latter is based on the classical approach deriving from the problem of an inclusion i in an infinite medium where phases are characterized by classes of crystallographic orientations.

$$\underset{\sim}{\boldsymbol{\sigma}}^i = \underset{\sim}{\boldsymbol{\Sigma}} + 2\mu\,(1-\beta)\left(\underset{\sim}{\boldsymbol{B}} - \underset{\sim}{\boldsymbol{\beta}}^i\right) \tag{19}$$

$$\beta = \frac{2\,(4-5\nu)}{15\,(1-\nu)} \tag{20}$$

$$\underset{\sim}{\boldsymbol{B}} = \sum f_i\, \underset{\sim}{\boldsymbol{\beta}}^i \tag{21}$$

$$\dot{\underset{\sim}{\boldsymbol{\beta}}}^i = \dot{\underset{\sim}{\boldsymbol{\epsilon}}}^{p,i} \overset{i}{-} D\,\epsilon_{eq}^{p,i}\,\underset{\sim}{\boldsymbol{\beta}}^i \tag{22}$$

where $\underset{\sim}{\boldsymbol{\sigma}}^i$ and $\underset{\sim}{\boldsymbol{\Sigma}}$ are respectively the inclusion and macroscopic stress tensors, μ is the macroscopic shear modulus and ν is the Poisson's ratio. The model introduces a macroscopic $\underset{\sim}{\boldsymbol{B}}$ and an inclusion $\underset{\sim}{\boldsymbol{\beta}}^i$ accomodation tensors. f_i is the inclusion volume fraction and D is the scale transition parameter. The equivalent Von Mises plastic strain of an inclusion is denoted by $\epsilon_{eq}^{p,i}$.

The identified parameters are given in Table 1. The numerical model shows a satisfactory agreement with both expermental quasi-static and cyclic material responses (Figure 1). Note that the negative value of the isotropic hardening parameter Q reflects the cyclic softening behaviour of the AISI H11 martensitic steel.

Table 1: Identified material parameters

Elasticity			Flow rule		Isotropic hardening		Kinematic hardening	
E (GPa)	ν	τ_0 (MPa)	n	K (MPa.s^{-n})	Q (MPa)	b	c	d (MPa)
208	0.3	372	15	4	-10	1.05	4.95 10^5	1700
Interaction matrix								Scale transition
h_1	h_2	h_3	h_4	h_5	h_6	h_7	h_8	D
1.1	0.7	0.9	0.9	1.0	1.2	1.3	0.7	15

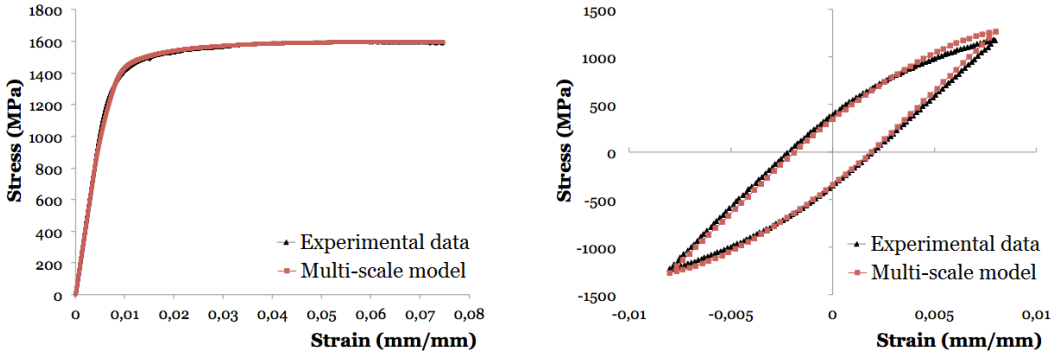

Figure 1: Material parameters identification (a) quasi-static uniaxial material response (b) cyclic material response

4 VIRTUAL MICROSTRUCTURE GENERATION

4.1 Martensitic structural characteristics

In order to investigated the full-field local mehanical behaviour, a virtual realistic microstructure of the AISI H11 has to be generated. The main martensitic microstructural charachteristics; i.e orientation and morphology; need to be accurately represented, since they have a significant role in understanding and predicting mechanical behaviour. As experimentaly outlined by sevral authors [10], product martensitic phase is related to the global coordinates through a former austenite grain orientation and variant orientations. The Kurdjumov-Sachs (KS) or Nishiyama-Wassermann (NW) α'/γ orientations relations are commonly used for lath martensitic steels; they are respectively defined as $(111)_\gamma \,//\, (011)_{\alpha'}$, $[\bar{1}01]_\gamma \,//\, [\bar{1}\bar{1}1]_{\alpha'}$ and $(111)_\gamma \,//\, (011)_{\alpha'}$, $[\bar{1}\bar{1}2]_\gamma \,//\, [0\bar{1}1]_{\alpha'}$. The other typical charachteristic consists in the complex structure morphology of laths. The experimental SEM and EBSD charachterization perfomed by Morito et al. [10] shows that martensitic laths sharing the same habit plane; i.e morphological parallel; are collected in packets which are the 'building' components of the former austenitic grain. The authors define also a block as a small group of laths with low angle misorientation which could be present in some cases.

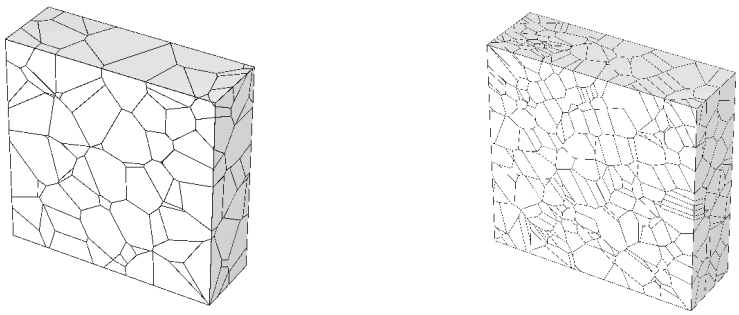

Figure 2: Virtual microstructure generation by Voronoï tesselations (a) martensitic potential packets (b) martensitic laths

4.2 Computational methodology

In the present investigation, Voronoï cells tesselations method is used to generate the virtual AISI H11 martensitic steel. The computational methodology consists first to perform ordinary Voronoï tesselations in a spatial domain of 150μm $\times$ 50μm $\times$ 150μm (Figure 2). The generated cells represent the potential sites of the martensitic packets (Figure 2(a)). From these tesselations, the former austenitic grains are defined as collections of groups of neighbors potential packets. Starting from these sites centers, randomely oriented segments are then generated where additional nucleation points are placed and second Voronoï tesselations are performed from these points. 1,034 polyhedra are generated and represent the martensitic laths which are the 'building' cells of the AISI H11 steel (Figure 2(b)). This computational methodology is consistent since it clearly highlights the morphological chacteristic of a martensitic microstructure from the collected parallel laths in packets to former austenitic grains. The second tesselations are physically analogous to martensitic transformation process where packets can grow through former austenitic grains boundaries. Furthermore, the present methodology avoids convex martensitic packets and former grains.

As an assumption, the Kurdjumov-Sachs (KS) orientations relation is adopted in the present investigation. The twenty four corresponding variants (Figure 3 (a)) are assigned to each austenitic former grain where each packet contains six variants sharing the same habit plane. A random isotropic orientations distribution is given to the former austenitic grains (Figure 3 (b)). In this manner, the product martensitic laths orientations distribution is isotropic (Figure 3 (c)).

5 FINITE ELEMENT COMPUTATIONS

5.1 Meshing and boundary conditions

Uniaxial quasi-static material response is investigated in the present work. Kinematic uniform boundary conditions type with a macroscopic strain of 8% are applied to the virtual microtructure in such a way that the microstructure is assumed to be placed at the

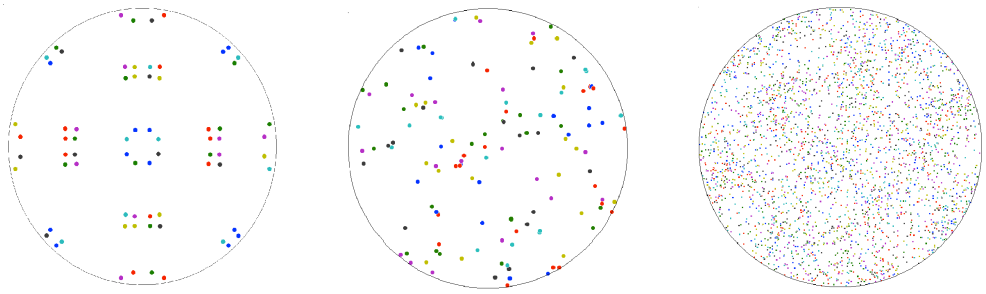

Figure 3: (100) pole figures (a) Kurdjumov-Sachs (KS) orientation relations (b) former austenitic grains (c) martensitic laths

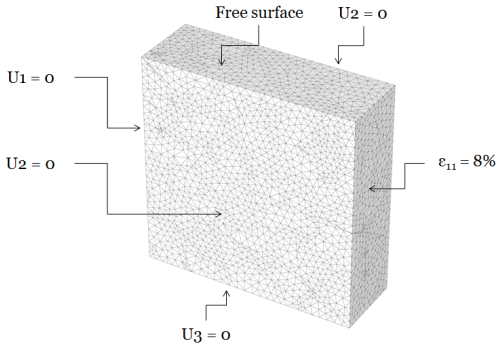

Figure 4: Virtual microstructure meshing and boundary conditions

surface of the specimen (Figure 4). A free-meshing technique is used to the above Voronoï tesselations [11]. The domain is discretized by about 85,000 second order tetrahedral finite elements (Figure 4).

5.2 Results

The finite element computations emphasize the heterogeneous and anisotropic nature of the local mechanical fields. As espected, the Von Mises stress concentrations fields are found at packets and laths boundaries (Figure 5). These localization fields are associated to preferential important plastic strain concentrations. However, the used stress-strain formulation shows effects on these concentration fields. Three localization regions corresponding to potential preferential paths in the virtual microstructure are invetigated.

The first region is highly solicited in the case of small strain assumption. The corresponding Von Mises equivalent plastic strain fields localization is quite important and homogeneous (Figure 6 (a)). The Von Mises stress fields are concentrated in packets and laths boudaries as mentioned above but they are more important than the neighboring areas (Figure 5 (a)). When the Olroyd objective stress rate is used, the first region is less solicited and the mechanical fields are more spread over the domain. The second region illustrates a higher concentration of the Von Mises equivalent plastic strain (Figure

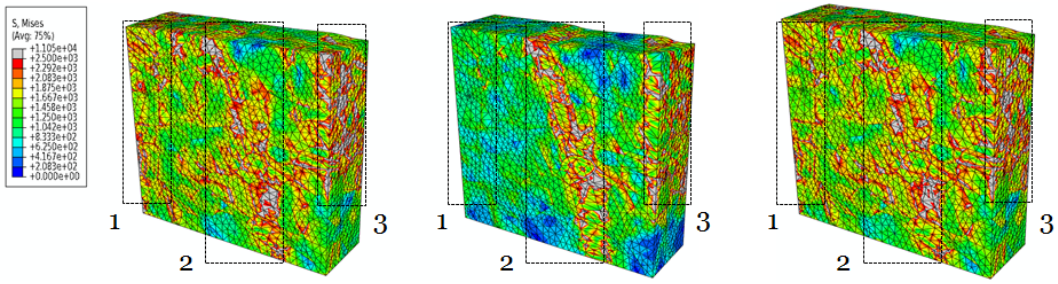

Figure 5: Von Mises equivalent stress contour maps (a) small strain assumption (b) Jaumann-Zaremba objective stress rate (c) Olroyd objective stress rate

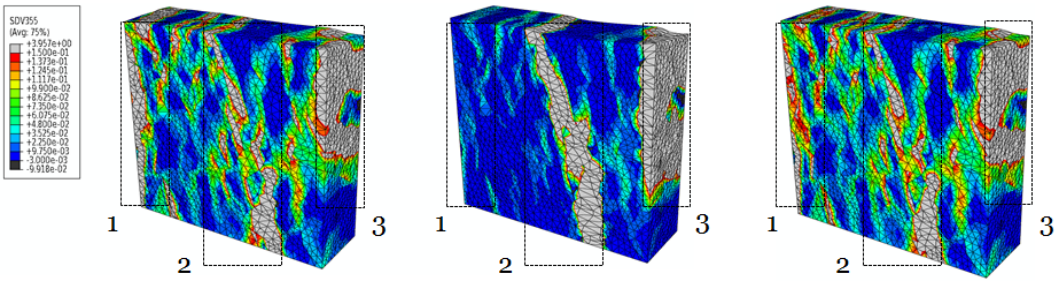

Figure 6: Von Mises equivalent plastic strain contour maps (a) small strain assumption (b) Jaumann-Zaremba objective stress rate (c) Olroyd objective stress rate

6 (c)) and corresponding stress (Figure 5 (c)) than the case of small strain assumption. However, in the case of Jaumann-Zaremba objective stress rate, the solicitaion of the first region is almost very low. The investigated domain shows a more homogeneous mechanical fields than the above cases with a strong concentration in the second and the third regions (Figure 6 (b)).

Figure 7 illustrates the contour maps of the number of activated slip systems. The distribution of activated slip systems is almost relevant with the one of the Von Mises equivalent plastic strain and corresponding stress. These contour maps reflect that the used stress-strain has an effect on the activation of a given slip system and thus on local mechanical fields. Furthermore, the obtained free surface profile depends also on the used stress-strain formulation. Figure 8 illustrates the normal strain contour maps at the free surface. It clearly emphasizes the difference between strain fields and the corresponding surface profile.

6 CONCLUSIONS

In this investigation, a numerical investigation was carried out on the heterogeneous and anisotropic mechanical behaviour of AISI H11 martensitic steel with a multi-scale approach. The elasto-viscoplastic model of Méric and Cailletaud [1] was implemented in the finite element code ABAQUS using three stress-strain formulations [5]: the small

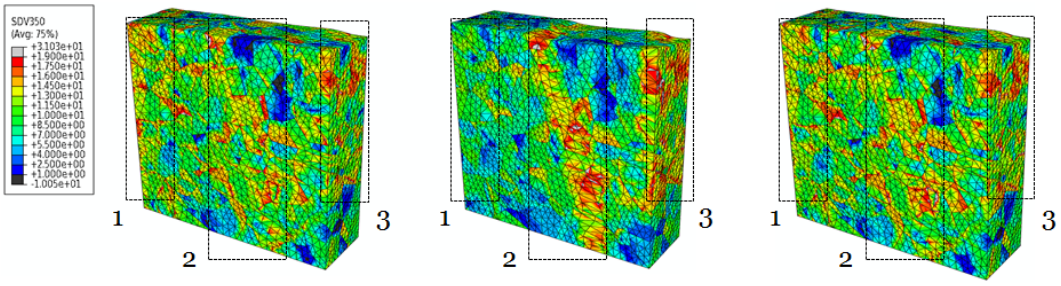

Figure 7: Number of activated slip systems contour maps (a) small strain assumption (b) Jaumann-Zaremba objective stress rate (c) Olroyd objective stress rate

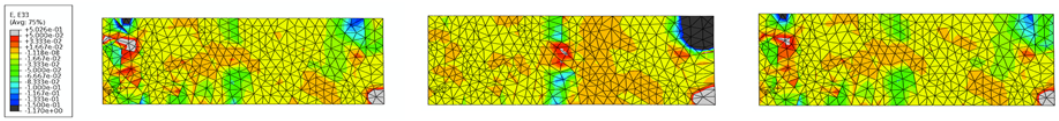

Figure 8: Normal strain contour maps at free surface (a) small strain assumption (b) Jaumann-Zaremba objective stress rate (c) Olroyd objective stress rate

strain assumption and two formulations based on finite strain theory which are respectively defined by the Jaumann-Zaremba and the Olroyd objective rates of Kirchhoff stress. The parameters of the model were identified using a mean field scale transition rule [6]. The local mechanical fields were investigated on a virtual microstructure generated by adapted Voronoï tesselations. The numerical investigation emphsizes the heterogeneous and anisotropic charachter of local mechanical fields. The results show that the stress-strain formulation has an impact on the localization of mechanical fields in such a way that preferential concentration paths of equivalent plastic strain and stress are quite different. So that, a particular attention should be paid to the used stress-strain formulation when mechanical fields localization is in concern.

REFERENCES

[1] Méric, L. and Cailletaud, G. Single crystal modeling for structural calculations. Part 2: Finite element implementation. *J. of Engng. Mat. Technol.* (1991) **113**:171–182.

[2] Mayeur, J.R. and Mcdowell, D.L. A three-dimensional crystal plasticity model for duplex Ti-6Al-4V. *Int. J. of Plasticity* (2007) **23**:1457–1485.

[3] Erieau, P. and Rey, C. Modeling of deformation and rotation bands and of deformation induced grain boundaries in IF steel aggregate during large plane strain compression. *Int. J. of Plasticity* (2004) **20**:1763–1788.

[4] Gérard, C., N'Guyen, F., Osipov N., Cailletaud, G., Bornert, M. and Caldemaison, D. Comparison of experimental results and finite elements simulation of strain

localization scheme under cyclic loading *Computational Materials Science* (2009) **46**:775–760.

[5] Hashiguchi, K. and Yamakawa, Y. *Introduction to Finite Strain Theory for Continuum Elasto-Plasticity*. Wiley, (2012).

[6] Pilvin, P. and Cailletaud, G. Utilisation de modèles polycristallins pour le calcul par éléments finis. *Revue Européene des Elements Finis* (1994) **3**:515–541.

[7] Franciosi, P. The concepts of latent hardening and strain hardening in metallic single crystals. *Acta Metallurgica* (1985) **33**:1601–1612.

[8] Ortiz, M. and Popov, E. P. Accuracy and stability of integration algorithms for elastoplastic constitutive relations. *Int. J. Numer. Meth. Engng* (1985) **21**:1839–1853.

[9] Peirce, D., Asaro, R.J. and Needlman, A. Material rate dependence and localized deformation in crystalline solids. *Acta Metallurgica* (1983) **31**:1951–1976.

[10] Morito, S., Huang, X., Furuharac, T., Makid, T. and Hansenb, N. The morphology and crystallography of lath martensite in alloy steels. *Acta Materialia* (2006) **54**:5323–5331.

[11] Quey, R., Dawson, P. R. and Barbe, F. Large-scale 3D random polycrystals for the finite element method: Generation, meshing and remeshing. *Computer Methods in Applied Mechanics and Engineering* (2011) **200**:1729–1745.